

Effect of Latex Volumetric Concentration on Void Structure, Particle Packing, and Effective Particle Size Distribution in a Pigmented Paper Coating Layer

Giuliano M. Laudone,[†] G. Peter Matthews,^{*,†} and Patrick A. C. Gané[‡]

Environmental and Fluid Modeling Group, University of Plymouth, Plymouth PL4 8AA, U.K., and Omya Development AG, CH-4665 Oftringen, Switzerland

A series of paper coating formulations was prepared by mixing calcium carbonate, ground to two particle size ranges, with latex binders of low and high glass transition temperature, each having different equivalent spherical particle diameters. These coating formulations were prepared by keeping the carbonate volume fraction constant, while the solids content in the mix was raised by the addition of the latex volume fraction. The viscosity of the coating formulations was measured by Brookfield viscometry. A disruption of particle packing in the wet phase, caused by the presence of the increasing latex volumetric concentration, was identified by viscosity measurements. The void structures of dry coating layers, prepared from the same mixes, were characterized by mercury porosimetry and were modeled using network simulation software that generates a simplified three-dimensional void network structure representative of the sample. The software model was also used to calculate the sizes of representative structural solid elements, which fit between the simulated voids, providing information not only of the pore space but also of the effective particle and/or agglomerate packing that generates that void space. Differences in the final dry structures of coating layers were observed and attributed to the disruption of the particle packing detected by the viscosity measurements.

Introduction

Pigmented coating layers are applied to paper to improve printability and optical properties. The coating is usually applied as an aqueous dispersion, or coating color, containing mineral pigments and binders. Industrially, the application of the coating color is carried out using a metered size press or a blade coater, which can reach speeds of about 2 000 m min⁻¹, and as a consequence, the rheological properties of the coating colors are of paramount importance. The coating is then dried under infrared dryers. The final printing and optical properties of the coating layers are closely related to their surface structure, void structure, and particle packing. In this study, observations on the viscosity of the coating formulations have been used to infer information about the particle packing in the wet phase and how this affects the dry coating layers in terms of pore space and structural solid elements.

Rheology. The rheological properties of coating color formulations have been the subject of many studies, mostly related to the runnability of the coating color under the very high speed of an industrial coater.^{1–3} The viscosity of low-concentration suspensions, consisting of rigid spherical particles, has been given by Einstein^{4,5} as

$$\eta_r = \frac{\eta}{\eta_0} = (1 + 2.5\phi) \quad (1)$$

where η_r is the relative viscosity defined as the ratio of the suspension viscosity, η , to the liquid-phase viscosity, η_0 , and ϕ ($=\phi_P + \phi_L$) is the volume fraction of the solid particles (pigment, P, plus latex, L). Therefore, according to this relation, the viscosity is seen to be proportional to the total volume fraction.

The interactions, packing, and flow behavior between latex and CaCO₃ in the coating color have been studied by Brookfield viscosity measurements. The aim of this study was to investigate how the latex particles and the CaCO₃ behave when mixed together in suspension and how their interaction is affected by the volumetric fraction of latex in the coating suspension.

A series of coating colors was prepared by mixing the slurried predispersed powder, as described in more detail in the next section, keeping the carbonate volume concentration constant while the solids content was raised by the addition of the latex volume fraction. The resultant measurement of Brookfield viscosity shows effectively how the latex particles in the coating color suspension gradually fill the gaps between the pigment particles and how this affects the packing interactions between latex and pigment particles. If the viscosity rises linearly over the initial range of latex addition, then it is possible to conclude that the latex particles are small enough to exist between the carbonate particles without disrupting their equilibrium packing and without establishing any other sorptive or chemical interaction. A deviation from the linear rise of the viscosity with the addition of latex implies that the latex is disrupting the mutual packing of the components or is taking part in some interparticle interaction.

Modeling. The Pore-Cor Research Suite software package (Environmental and Fluid Modeling Group, University of Plymouth, Plymouth, U.K.) provides a void network simulation and has been previously used to model a range of materials such as soil, sandstone, catalysts, and paper coating.^{6–10} It represents the void structure of a porous medium as a series of identical interconnected unit cells with periodic boundary conditions. Each unit cell comprises an array of 1 000 nodes equally spaced in a Cartesian cubic-close-packed array. Cubic pores are positioned with their centers at each node and are connected by cylindrical throats in each Cartesian direction.

A Boltzmann-annealed simplex⁸ is used to adjust four parameters so that the mercury intrusion curve of the simulated

* To whom correspondence should be addressed. E-mail: pmatthews@plymouth.ac.uk.

[†] University of Plymouth.

[‡] Omya Development AG.

structure closely matches that of the experimental sample. The four parameters are as follows:

- connectivity, defined as the average number of connected throats per pore, up to a maximum of six (one connected to every face of the cubic pore);
- throat skew, defined as the percentage of throats of the smallest size in a distribution of 100 sizes which is linearly distributed when plotted on a logarithmic size axis;
- pore skew, a scaling factor which bulks up the sizes of the pores to achieve the experimental porosity, up to and limited by the largest size already present in the size distribution; and
- correlation level, which sets the level of local size-autocorrelation of the features, in the present case giving rise to vertical banding within each unit cell.

The simplex also takes into account three Boolean parameters, namely, whether the network can be drawn with no features overlapping, whether it can be adjusted to the experimental porosity, and whether the network is unfragmented.

The model creates groups of stochastic realizations known as stochastic generations. Each stochastic generation of the structure is created by using a set of pseudorandom starting numbers, with each set being different. If the unit cell is the same size as the representative elementary volume (REV) of the sample, and its complexity of its geometry is sufficient to represent the geometric complexity of the experimental void structure, then different stochastic generations will all have the same properties, as the random effects will average out across the unit cell. Usually the model does not fulfill the criteria of representing the REV of the sample, and the variability of the results for different stochastic generations must be analyzed statistically. However, it has been shown by Schoelkopf et al.⁶ that, in the modeling of paper coating, the properties of different stochastic generations are similar because the REV, in terms of coating thickness, is similar to the actual size of the unit cell.

Within the porous network structure generated to simulate the void space of a porous sample, the software has been developed to generate spherical "skeletal elements", which are representative of the solid phase of the porous material. The algorithm used to calculate the size of the skeletal elements has been fully described by Mathews et al.¹¹ Spherical skeletal elements are grown from the center of the space between eight cubic pores until they touch the corners of up to four pores. In this previous publication, the algorithm is validated against unconsolidated sand samples, showing simulated skeletal element sizes matching the experimental particle size distributions of the sand samples. The algorithm has already been modified and used to simulate the skeletal element size distributions of paper coating layers.¹²

Experimental Section

Materials. The pigment was a wet-ground predispersed calcium carbonate powder from Orgon, France, ground to two particle size ranges, which we refer to as gcc60 and gcc90 (Hydrocarb 60 and 90 from Omya AG, CH-4665 Oftringen, Switzerland). The samples contained, respectively, 60 w/w% and 90 w/w% of particles with diameter $< 2 \mu\text{m}$ and with a maximum diameter of $\sim 5 \mu\text{m}$.¹³ The carbonate suspensions also contained small amounts of polyacrylate-based dispersant.

The binder for each sample was selected from one of the following:

- high glass transition temperature ($T_g = 23 \text{ }^\circ\text{C}$) acrylic latex Acronal S320D (BASF, Germany) in the form of spherical particles of diameter $0.2 \mu\text{m}$;

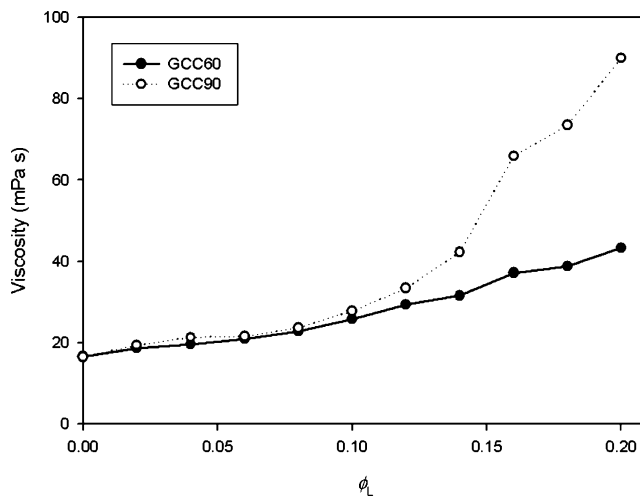


Figure 1. Brookfield viscosity at 22 s^{-1} shear rate for calcium carbonate and increasing volumetric fractions, ϕ_L , of acrylic high T_g latex.

- high T_g ($22 \text{ }^\circ\text{C}$) styrene–butadiene latex DL940 (Dow Chemicals, U.S.A.) with spherical particles of diameter $0.14 \mu\text{m}$;
- low T_g ($5 \text{ }^\circ\text{C}$) styrene–butadiene latex DL930 (Dow Chemicals, U.S.A.) with spherical particles of diameter $0.15 \mu\text{m}$.

Samples. The volumetric fraction of mineral pigment was kept constant ($\phi_P = 0.2$), while the volumetric fraction of latex (ϕ_L) was increased from 0 (suspensions of CaCO_3 only) to 0.2 by the addition of latex to preprepared CaCO_3 slurries.

Coating layers, with 10 w/w% and 25 w/w% of binder, respectively, were applied onto aluminum foil. The latex volumetric concentration for these formulations was about $\phi_L = 0.06$ and $\phi_L = 0.18$, respectively. The total solid content of these formulations was 55 w/w%. This is equal to the total solid content of the formulations with the highest volumetric concentration used for the Brookfield viscosity measurements. Two different coating weights for each formulation were applied (10 g m^{-2} and 20 g m^{-2}), and the coating layers were dried at room temperature.

The dry coating samples were analyzed by mercury porosimetry,¹⁴ using an Autopore III instrument (Micromeritics, Norcross, GA).

The results of the mercury intrusion porosimetry measurements were corrected for sample compression using the Pore-Comp application within the Pore-Cor Research Suite package, which applies the equations presented by Gane et al.¹⁵ and calculates the corrected mercury intrusion curve and the bulk modulus of the samples.

Results

Brookfield Viscosity. The results are shown in Figures 1–3. It can be observed that the measured values of Brookfield viscosity (HA1 spindle at 100 min^{-1} , corresponding to a shear rate of 22 s^{-1}) for gcc60- and gcc90-based coating colors are similar at low latex volumetric fractions, when the same latex is used, and that the increase in viscosity is almost linear with the volumetric concentration of binder in the suspension. This confirms that no significant interaction of a chemical nature is occurring between the latices and the pigments. In the case of gcc60, this linear increase in viscosity continues throughout the range of binder volumetric concentration investigated, as can be observed in Figures 1–3. However, in the case of gcc90-based coating colors, when the latex volumetric fraction reaches

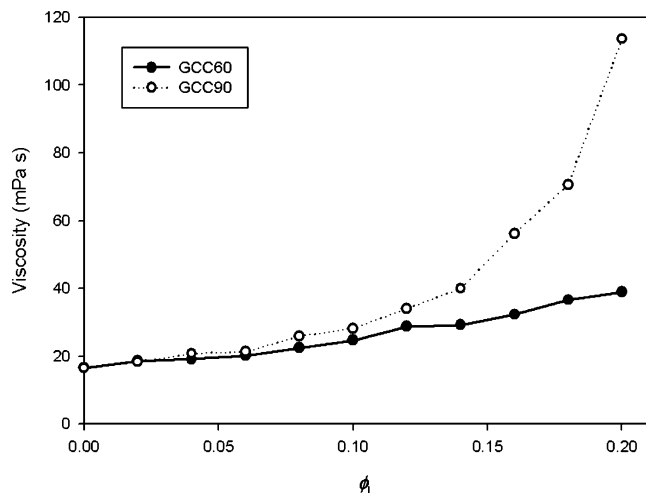


Figure 2. Brookfield viscosity at 22 s^{-1} shear rate for calcium carbonate and increasing volumetric fractions, $\phi_{L,r}$ of styrene-butadiene high T_g latex.

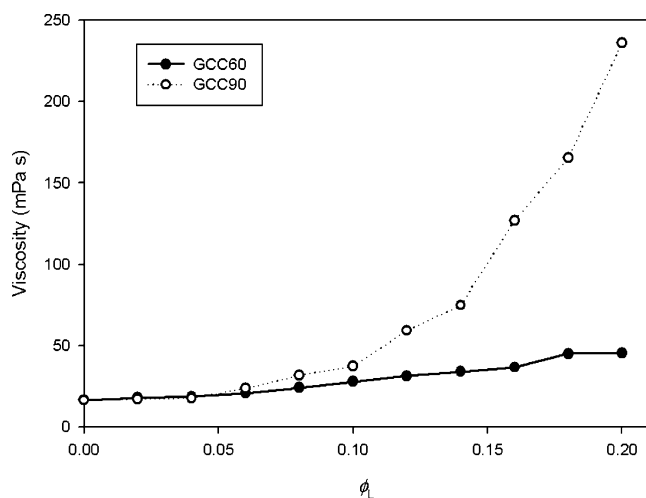


Figure 3. Brookfield viscosity at 22 s^{-1} shear rate for calcium carbonate and increasing volumetric fractions, $\phi_{L,r}$ of styrene-butadiene low T_g latex.

a value of 0.10–0.15, a steeper rise of the viscosity of the suspension can be observed. Thus, it can be deduced that the finer pigment, with its tighter packing per unit solids content, is more easily disrupted by the addition of latex once the latex level rises to a volume fraction of 0.10–0.15.

It is also interesting to observe that the values of Brookfield viscosity measured for different types of latex, when the same pigment was used, were all of the same order of magnitude, independent from the chemical formulation and the film-forming properties of the latex. The only exception to this (Figure 3) is the styrene-butadiene low T_g with gcc90 at high volumetric fractions of latex, which shows a higher value of viscosity.

Mercury Porosimetry. The porosities of the dry samples, measured as described above, are shown in Table 1, and the mercury intrusion porosimetry curves are shown in Figures 4–7. The porosities are plotted as 0–100% of total accessible void volume, and the applied pressures have been converted

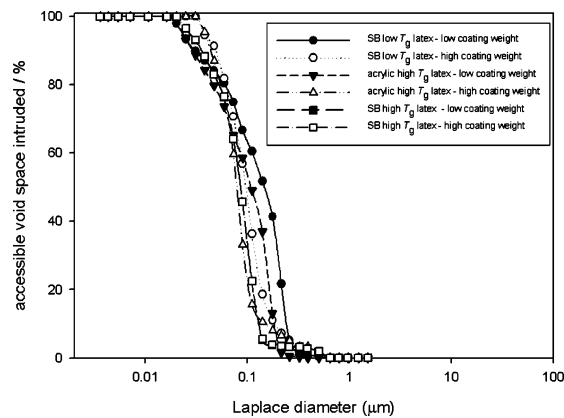


Figure 4. Mercury intrusion porosimetry for gcc90 + 10 w/w% latex samples.

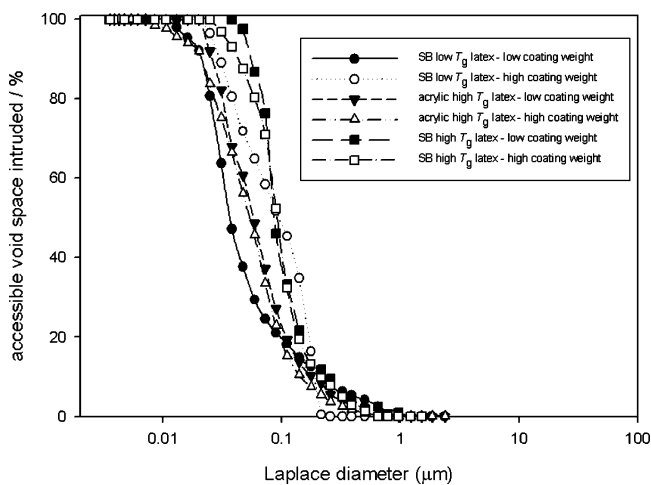


Figure 5. Mercury intrusion porosimetry for gcc90 + 25 w/w% latex samples.

to sizes using the Laplace equation

$$D = \frac{-4\gamma \cos \theta}{p} \quad (2)$$

where γ is the interfacial tension between mercury and air (0.485 Nm^{-1}), p is the applied pressure, and θ is the contact angle (assumed to be 140°). Uncertainties in these parameters are discussed by Van Brakel et al.¹⁶

The curves shown in Figures 4–7 were used as the input data for the pore network model described above. The model fitted the shape of each entire mercury intrusion curve and matched the porosity of each sample to 0.01% of the total sample volume.

Modeling. The skeletal element size distributions for the paper coating layers were subsequently generated with the algorithm previously described. For each paper coating formulation, different stochastic realizations and, as a consequence, different size distributions have been generated. These have also been compared by the Mann–Whitney statistic test,¹⁷ and

Table 1. Porosities of Dry Samples Measured by Mercury Porosimetry

sample	acrylic high T_g latex (low coating wt)	acrylic high T_g latex (high coating wt)	SB high T_g latex (low coating wt)	SB high T_g latex (high coating wt)	SB low T_g latex (low coating wt)	SB low T_g latex (high coating wt)
gcc60 + 10% binder	26.1	24.8	30.8	25.8	21.8	18.7
gcc60 + 25% binder	19.8	18.9	24.2	19.6	14.2	12.8
gcc90 + 10% binder	38.4	24.5	39.9	32.2	28.5	24.9
gcc90 + 25% binder	37.7	23.2	35.1	21.9	15.5	13.9

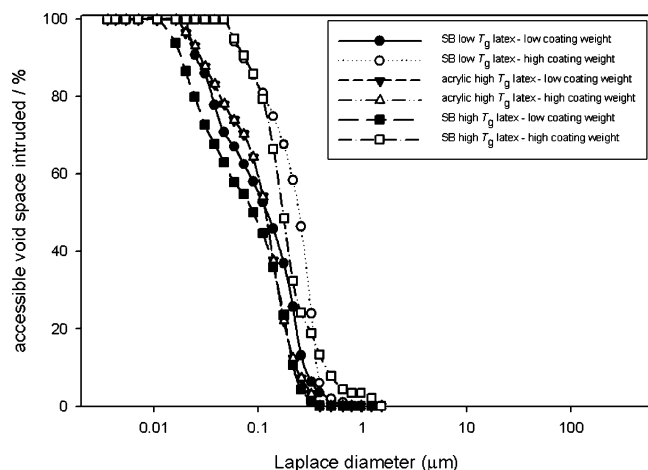


Figure 6. Mercury intrusion porosimetry for gcc60 + 10 w/w% latex samples.

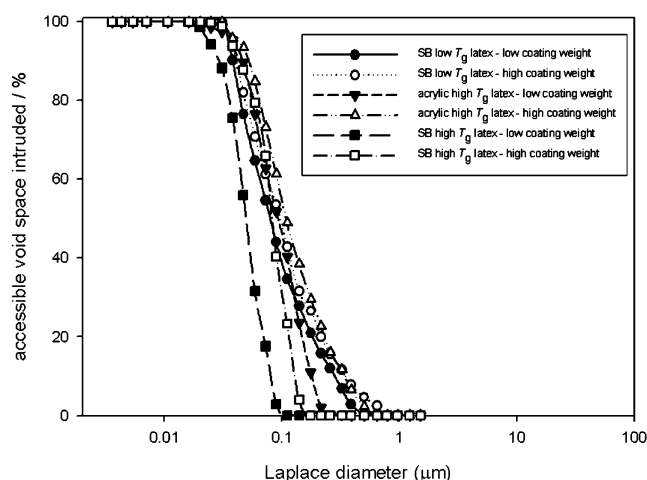


Figure 7. Mercury intrusion porosimetry for gcc60 + 25 w/w% latex samples.

all showed a value of P larger than 0.05. This means that the different stochastic realizations of the structures give skeletal element size distributions that are statistically equal to each other. Hence, the results presented below show only the size distribution for one stochastic realization for each coating color formulation. The results of statistical tests on the skeletal element size distributions of different coating color formulations can be taken as $P = 0$ (i.e., the skeletal element size distributions are statistically different) unless otherwise stated.

The skeletal element algorithm generates 1 000 particles which can be represented as distributions, as shown in Figure 8 for a gcc90 with 25 w/w% low T_g latex. To limit the number of figures presented in this article, the distributions are summarized in Tables 2 and 3 as maximum, minimum, and average skeletal element sizes. A more-detailed representation of these simulation results and their sensitivity analyses can be found in Laudone et al.¹²

The three-dimensional representations of simulated unit cells are shown in Figure 9. It represents the void space and the skeletal elements of a gcc90 with styrene-butadiene low T_g latex.

Tables 2 and 3 show the results of the skeletal element size distribution calculation for the paper coating layers based on calcium carbonate and, respectively, 10 w/w% and 25 w/w% of latex.

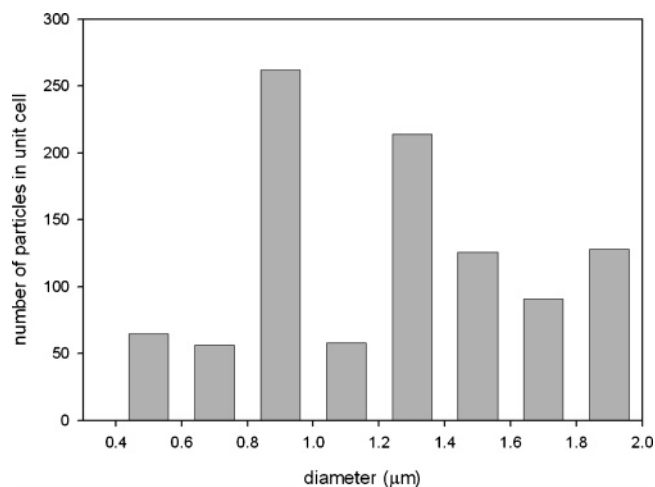


Figure 8. Skeletal element size distribution in a paper coating layer of gcc90 + 25 w/w% low T_g latex.

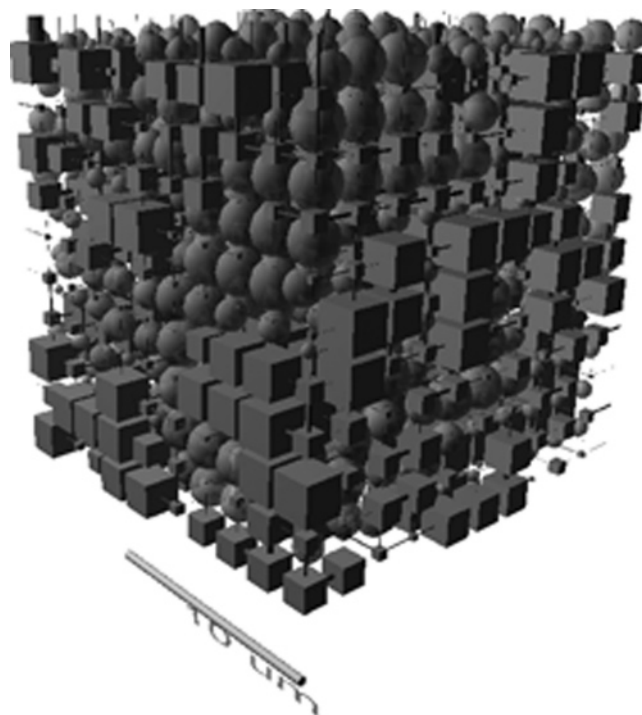


Figure 9. Three-dimensional representation of a unit cell with skeletal elements generated between the pores for a low coat weight sample of gcc90 + 25 w/w% styrene-butadiene low T_g latex. The distribution of the skeletal elements size for this sample can be found in Figure 8.

Discussion

The drying process of a paper coating layer has been described by Watanabe and Lepoutre¹⁹ as divided into three phases. During the first phase, water evaporates at the liquid-air interface. At the first critical concentration (FCC), a three-dimensional network is formed and particle motion is greatly restricted. During the second phase, shrinkage of the porous network occurs under the driving action of surface capillary forces. At the second critical concentration (SCC), the network is fixed and air enters the rigid structure as the liquid retreats.

It is important to take the relationship between particle-particle interaction in the wet phase and the size of the skeletal elements in the dry structure of the coating layer into account. We have observed that the wet-phase interaction (rheology) seems to strongly affect the dry structure at the SCC. The structure of the coating color at the intermediate FCC must also,

Table 2. Minimum, Maximum, and Average Modeled Skeletal Element Diameter for gcc90-Based Coating Layers

skeletal element size/ μm	10 w/w% binder low coating weight			10 w/w% binder high coating weight			25 w/w% binder low coating weight			25 w/w% binder high coating weight		
	min	avg	max	min	avg	max	min	avg	max	min	avg	max
acrylic high T_g latex	0.02	0.24	1.53	0.89	1.30	2.04	0.08	0.31	1.02	0.58	0.75	1.13
SB high T_g latex	0.24	0.55	1.66	0.40	0.80	1.75	0.29	0.55	1.69	0.22	0.88	1.72
SB low T_g latex	0.77	1.34	1.96	0.85	1.39	2.01	0.40	1.22	1.75	0.14	1.23	1.90

Table 3. Minimum, Maximum, and Average Modeled Skeletal Element Diameter for gcc60-Based Coating Layers

skeletal element size/ μm	10 w/w% binder low coating weight			10 w/w% binder high coating weight			25 w/w% binder low coating weight			25 w/w% binder high coating weight		
	min	avg	max	min	avg	max	min	avg	max	min	avg	max
acrylic high T_g latex	0.75	1.38	1.95	1.02	1.50	2.11	0.52	1.26	1.82	0.90	1.47	2.05
SB high T_g latex	0.33	0.93	1.71	0.96	1.31	2.08	0.43	0.83	1.77	0.09	0.89	1.57
SB low T_g latex	0.43	1.30	2.12	1.19	1.56	2.21	0.69	1.29	1.92	0.52	1.31	2.21

therefore, be a direct consequence of the rheology of the system, in particular the particle–particle interactions and the disruption of the particles packing in the wet phase.

As we have now seen, using the method of volume fraction, it is possible to determine rheologically the point at which there is an onset of packing or interactive disruption as latex is added to calcium carbonate. In the case of the coarse pigment gcc60, there is apparently sufficient space between the pigment particles to allow for the additional volume fraction of latex without any additional disruption of the equilibrium packing properties at the given pigment volume fraction, i.e., viscosity is a simple function of total volume fraction content including latex. Consequently, during the drying of such a mixture, it is expected that the structure will maintain similarity throughout the drying process if the process only involves the removal of water. This assumes that concentration of soluble species will have only a minor role to play.

In the case of the finer gcc90, on the other hand, higher volume fractions of latex induce a packing disorder or interaction with the pigment. This could be argued purely on the basis of particle packing or could be due to other interactions. From this test it is not possible to determine the exact nature of the interaction, though it is interesting to see that the low T_g styrene–butadiene latex generates the most interaction. Given that the chemistry of the two carbonate pigments is essentially the same, it is unlikely that the interaction is chemical, and we can assume that the rise in viscosity on addition to the gcc90 is most likely to be due to packing. Latex surface chemistry could affect the latex–carbonate and latex–latex interactions, but this would affect the viscosity curves over the whole range of latex addition. Figures 1–3 show that the Brookfield viscosity changes occur only above a certain threshold, which suggests that this effect is most likely to be caused by packing disruption.

The particle sizes of the different latices range from 0.14 for the SB high T_g latex to 0.2 μm for the acrylic high T_g latex. Gcc90 has an average particle size, in terms of number percent of particles, of $\sim 0.1 \mu\text{m}$, while gcc60 has an average particle size of $\sim 0.5 \mu\text{m}$. The latex particles are, therefore, of the same size or are larger than the average gcc90 particle, and this will obviously have a strong tendency toward disruption of the calcium carbonate packing. In the case of gcc60, the latex particles are smaller than the average carbonate particle and are not so likely to cause disruption of the packing.

Once the packing disruption occurs, it is likely that the latex will play a very important role in determining the packing behavior difference between that of a coating color, containing pigment and latex, compared with the pure slurry of pigment alone as solids rise during the drying. The final properties of the dry coating layer will, thus, be strongly dependent on the

latex particle size and physical properties, such as glass transition temperature, T_g , as well as any physicochemical interactions that might be taking place.

The results of the skeletal elements modeling (Tables 2 and 3) show that, as expected, the skeletal elements for the gcc60-based coating layers are larger than those in a gcc90-based coating layer in nearly every case. It can be also seen that the thickness of the coating layer affects significantly the skeletal element size distribution, with thicker coating layers (higher coating weights) showing larger skeletal elements, and results in finer void space pores. This observation is in agreement with the noted decrease in porosity as coating thickness increases,^{14,18} with the porosity loss being partly compensated for in the model by larger skeletal elements. It also appears that the amount of nonfilming (high T_g) acrylic binder in the coating color formulations does not cause an increase in skeletal element size. In the case of coarse calcium carbonate, the size distribution for 10 w/w% and 25 w/w% of binder in a thick coating layer is identical ($P = 0.062$). The same trends can be observed when the high T_g latex used has a different chemical formulation.

The low T_g filming of latex affects the size distribution of the skeletal elements: Tables 2 and 3 show larger skeletal elements both in the minimum and maximum size ranges when compared to high T_g latices. The use of a coarser pigment leads to larger skeletal elements, and an increasing amount of applied coating color also leads to larger skeletal elements.

The amount of low T_g binder does not seem to affect the size of the skeletal elements in the case of the gcc60, and with a thin coating layer, the two distributions are statistically very similar ($P = 0.082$). This suggests that the coating is constrained in its shrinkage behavior due to the larger pigment particle size.

There is no obvious relationship between the size of the structural elements and the porosity of the samples when compared between different samples. For example, in the case of gcc60, there is a similarity of the sizes of structural elements between the high T_g acrylic latex and low T_g SB in Tables 2 and 3 (for example 10% binder at high coat weight) when there is a large difference in the total porosity (Table 1) between the two formulations. This means that the sizes of the elements do not necessarily trend with porosity, as similar sized elements can pack closer together in one case versus the other.

When high T_g latex is used as binding agent, the size of the skeletal element is smaller than in the case of low T_g latex. This suggests that the latex particles do not film-form during drying under the experimental conditions and stay as hard spheres. On the other hand, low T_g latex particles either film-form upon drying or become extruded or intruded into the porous structure under the forces experienced during drying.

These processes give rise to expectedly larger skeletal elements and effectively block off access to smaller pores.

The observed increase in sizes of skeletal elements with the thickness of the coating layer can be explained by taking into account the freedom of rearrangement of the particles of pigment and binder upon drying of the coating layer. As the coating layer dries, the particles of binder and pigment will rearrange. When a higher weight, thicker coating layer is applied on the substrate, the particles have more space available for rearrangement. They are no longer being constrained in the z direction normal to the surface plane of the sheet by the presence of the large particles, which in the case of lower coating weights are themselves as big as the coating layer itself. This freedom of rearrangement will result in a highly packed structure, as shown by lower values of porosity, with a larger number of ultrafine features, pores and throats. The simple geometric representation of the void space and of the solid phase of the porous material, used by the network simulation software, cannot take into account such ultrafine void features, and therefore, the final results show larger solid elements.

The correlation between the sizes of the skeletal elements in the final dry structure and the rheological properties in the wet color appears even clearer in the case of low T_g latex-based formulations. Figure 3 shows that the interactions between gcc60 and low T_g latex are slightly stronger than in the case of high T_g latex (Figures 1 and 2), and as a consequence, the skeletal elements shown in Table 3 for low T_g latex-based coatings are only slightly larger than in the cases of high T_g latex-based coatings. Figure 3, on the other hand, also shows that the interaction between the finer gcc90 carbonate and the low T_g latex particles are far larger than those observed for high T_g latex. This, as expected, results in average skeletal element sizes between 40% and 120% larger for the gcc90 with low T_g latex-containing color than those modeled for gcc90 with high T_g latex (Table 2).

Conclusions

In this study, it has been shown that the viscosity of CaCO_3 and latex suspensions follows the Einstein equation at low volumetric concentration of latex. The interactions between particles of finer calcium carbonate, at constant pigment volume fraction, and latex are interpreted as a disruption of packing by the presence of the increasing latex volumetric concentration, which results in a deviation of the viscosity values from Einstein's linear equation.

Differences in the final dry structures of coating color formulations have been linked with this disruption and the resulting changes in viscosity, together with an effect caused by the thickness of the coating layer. The simulated skeletal element size distributions showed significant differences which supported these observations.

Literature Cited

(1) Triantafillopolous, N. *Paper Coating Viscoelasticity—And Its Significance to Blade Coating*; Tappi Press: Atlanta, GA, 1996.

(2) Husband, J. C. Interactions between ground calcium carbonate pigments and polymer latices. *Nord. Pulp Pap. Res. J.* **2000**, *15*, 382–386.

(3) Gane, P. A. C. Relaxation-induced dilatancy in separable viscoelastic suspensions: Proposing a novel rheological phenomenon. *1997 Tappi Advanced Coating Fundamentals Symposium*; Tappi Press: Atlanta, GA, 1997.

(4) Einstein, A. Eine neue Bestimmung der Moleküldimensionen. *Ann. Phys. (Leipzig)* **1906**, *19*, 289–306.

(5) Einstein, A. Berichtigung zu meiner Arbeit: "Eine neue Bestimmung der Moleküldimensionen". *Ann. Phys. (Leipzig)* **1911**, *34*, 591–592.

(6) Schoelkopf, J.; Ridgway, C. J.; Gane, P. A. C.; Matthews, G. P.; Spielmann, D. C. Measurement and network modelling of liquid permeation into compacted mineral blocks. *J. Colloid Interface Sci.* **2000**, *227*, 119–131.

(7) Bodurtha, P.; Matthews, G. P.; Kettle, J. P.; Roy, I. M. Influence of Anisotropy on the Dynamic Wetting and Permeation of Paper Coatings. *J. Colloid Interface Sci.* **2005**, *283*, 171–189.

(8) Johnson, A.; Roy, I. M.; Matthews, G. P.; Patel, D. An Improved Simulation of Void Structure, Water Retention and Hydraulic Conductivity in Soil, Using the Pore-Cor Three-Dimensional Network. *Eur. J. Soil Sci.* **2003**, *54*, 477–489.

(9) Matthews, G. P. Computer Modelling of Fluid Interactions in Porous Coatings and Paper—An Overview. *Nord. Pulp Pap. Res. J.* **2000**, *15*, 422–430.

(10) Ridgway, C. J.; Gane, P. A. C.; Schoelkopf, J. Modified Calcium Carbonate Coatings with Rapid Absorption and Extensive Liquid Uptake Capacity. *Colloids Surf., A* **2004**, *236*, 91–102.

(11) Mathews, T. J.; Matthews, G. P.; Huggett, S. Estimating Particle Size Distributions From a Network Model of Porous Media. *Powder Technol.* **1999**, *104*, 169–179.

(12) Laudone, G. M.; Matthews, G. P.; Gane, P. A. C.; Ridgway, C. J.; Schoelkopf, J. Estimation of the effective particle sizes within a paper coating layer using a void network model. *Chem. Eng. Sci.* **2005**, *60*, 6795–6802.

(13) Laudone, G. M.; Matthews, G. P.; Gane, P. A. C. Observation of Shrinkage during Evaporative Drying of Water-Based Paper Coatings. *Ind. Eng. Chem. Res.* **2004**, *43*, 712–719.

(14) Laudone, G. M.; Matthews, G. P.; Gane, P. A. C. Coating Shrinkage during Evaporation: Observation, measurement and modelling within a network structure. *2003 Advanced Coating Fundamentals Symposium*; TAPPI Press: San Diego, CA, 2003.

(15) Gane, P. A. C.; Kettle, J. P.; Matthews, G. P.; Ridgway, C. J. Void Space Structure of Compressible Polymer Spheres and Consolidated Calcium Carbonate Paper-Coating Formulations. *Ind. Eng. Chem. Res.* **1996**, *35*, 1753–1764.

(16) Van Brakel, J.; Modry, S.; Svata M. Mercury Porosimetry: State of the Art. *Powder Technol.* **1981**, *29*, 1–12.

(17) Dancy, C. P.; Reidy, J. *Statistics without Maths for Psychology—Using SPSS for Windows*, second ed.; Prentice Hall: New York, 2002; p 517.

(18) Xiang, Y.; Bousfield, D. Effect of Coat Weight and Drying condition on Coating Structure and Ink-Setting. *2001 Advanced Coating Fundamentals*; TAPPI Press: San Diego, CA, 2001.

(19) Watanabe, J.; Lepoutre, P. A Mechanism for the Consolidation of the Structure of Clay–Latex Coatings. *J. Appl. Polym. Sci.* **1982**, *27*, 4207–4219.

Received for review November 22, 2005
Revised manuscript received January 12, 2006
Accepted January 13, 2006

IE051301Q